Calibrated Waveform Measurement With High-Impedance Probes

Pavel Kabos, *Senior Member, IEEE*, Howard Charles Reader, Uwe Arz, *Member, IEEE*, and Dylan F. Williams, *Fellow, IEEE*

***Abstract*—We develop an on-wafer waveform calibration technique that combines a frequency-domain mismatch correction to account for the effects of the probe on the measurement with an oscilloscope calibration. The mismatch correction is general and can be applied to any type of microwave probe, including scanning and internal-node probes for noninvasive integrated-circuit tests. We show that, for the commercial high-impedance probe we used, this calibration approach allows accurate on-wafer waveform reconstruction for a variety of probe ground configurations.**

***Index Terms*—Calibration, high-impedance probe, on-wafer measurement, waveform measurement.**

I. Introduction

WE HAVE developed a calibration for on-wafer waveform measurements performed at the internal nodes of an integrated circuit with a high-impedance probe and an oscilloscope. The calibration relies on a mismatch correction based on the broad-band frequency-domain probe-characterization method introduced in [1] and on a separate oscilloscope calibration. The calibrations account for the finite impulse response of the oscilloscope, signal distortion in the probe, and multiple reflections between the probe and oscilloscope.

The goal of internal-node probing and field mapping is to measure voltage and/or current waveforms at different locations within digital or microwave integrated circuits. A number of broad-band probes with low invasiveness have been developed for this task. Common approaches include electrooptic probes [2], photoconductive probes [3]–[5], microwave microelectromechanical system (MEMS) probes [6], and commercial microwave probes [7], [8].

Most optical, and some micromechanical probes, incorporate waveform measurement systems directly in the probes and cannot be characterized directly with the method developed here. However, a broad class of passive and active microwave probes, including those described in [6]–[8], can be treated as standard two-port microwave devices, and can be characterized with the method of [1].

Manuscript received March 22, 2002.

P. Kabos and D. F. Williams are with the National Institute of Standards and Technology, Boulder, CO 80305 USA (e-mail: kabos@boulder.nist.gov; dylan@boulder.nist.gov).

H. C. Reader was with the National Institute of Standards and Technology, Boulder, CO 80305 USA. He is now with the Electrical and Electronic Engineering Department, University of Stellenbosch, Stellenbosch, Matieland 7602, South Africa.

U. Arz was with the University of Hanover, 30060 Hanover, Germany. He is now with the Physikalisch-Technische Bundesanstalt, 38116 Braunschweig, Germany.

Digital Object Identifier 10.1109/TMTT.2002.807842

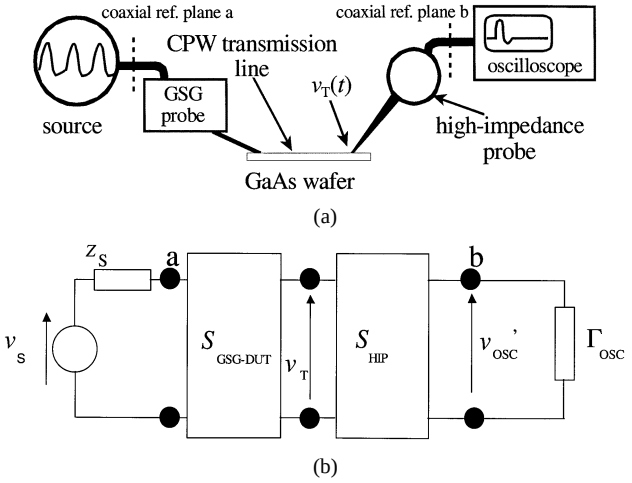

Fig. 1. Our experimental apparatus, on-wafer CPW transmission lines, and the equivalent circuit used to develop our mismatch corrections.

Here, we develop an on-wafer waveform calibration method for measurement systems consisting of an oscilloscope and a passive or active microwave probe characterizable with the method of [1]. The calibration combines a novel mismatch correction with previously developed oscilloscope calibrations. We show that the calibration works well even when the probes have a ground contact that can either be arbitrarily positioned on the circuit or not used at all [7].

II. Waveform Measurements

Fig. 1(a) shows a sketch of our experimental apparatus. The source on the left-hand side drives the input of a conventional ground–signal–ground (GSG) microwave probe. This probe has a low loss and a nominal impedance of 50 Ω. While the method is applicable to any type of signal source, in our experiments, we used a comb generator that creates a distorted 800 MHz sine wave rich in harmonics at its nominally 50-Ω coaxial output.

The GSG probe just to the right-hand side of the source injects the signal from the source's coaxial output port into a coplanar waveguide (CPW) transmission line printed on a gallium arsenide (GaAs) substrate. The goal of the experiment is to accurately measure the waveform $v_{\rm T}(t)$ at the right-most end of the CPW transmission line, as illustrated in Fig. 1(a), with the high-impedance probe and oscilloscope. Here, the subscript "T" indicates that the voltage in the CPW we wish to measure is near the tip of the high-impedance probe. To measure the waveform $v_{\rm T}(t)$, we contacted the CPW center conductor near its end with the high-impedance probe. The probe transmitted the signal at

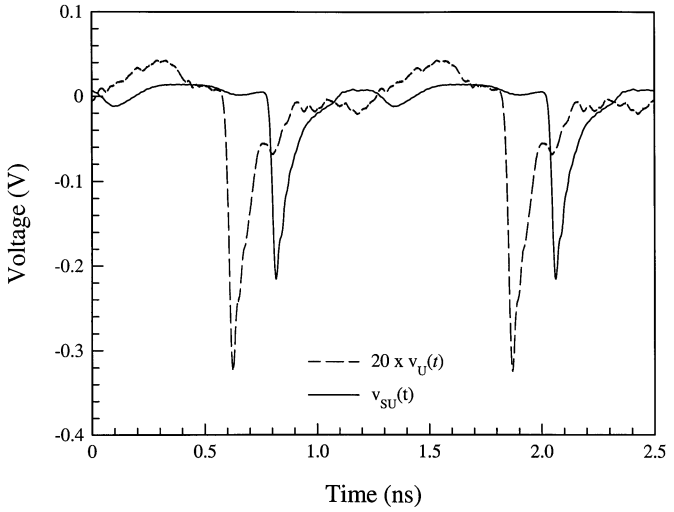

Fig. 2. Comparison of the voltage v_{SU} measured at the source and 20 times v_{U}, the voltage generated by the source at the coaxial port of the high-impedance probe.

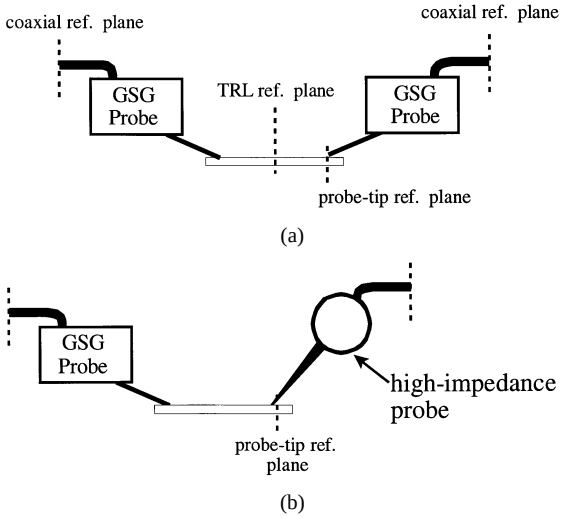

Fig. 3. Sketch of the two measurement configurations employed in the probe characterization procedure of [1].

its tip to the sampling oscilloscope at the right-hand side of the figure. The probe we used was equipped with a movable ground contact that could be connected to either of the CPW grounds, or not connected at all, and a 950-Ω resistor integrated in its tip to reduce its invasiveness. The oscilloscope had a 50-GHz bandwidth and a nominal input impedance of 50 Ω at its coaxial port.

III. Waveform Distortion

Fig. 2 plots the uncalibrated voltage $v_{\mathrm{SU}}(t)$ measured at the coaxial reference plane a of Fig. 1(a) at the output of our source as a solid line. This figure compares $v_{\mathrm{SU}}(t)$ to 20 $v_{\mathrm{U}}(t)$, where v_{U} is the uncalibrated voltage we measured at the coaxial reference plane b of Fig. 1(a) at the output of the high-impedance probe after the signal from the source has propagated through the 50-Ω GSG probe, coplanar line, and high-impedance probe, as illustrated in Fig. 1. The factor of 20 accounts for the expected attenuation of the signal due to the 950-Ω series resistor integrated into the tip of the high-impedance probe.

The voltage waveforms in Fig. 2 illustrate key problems of this time-domain measurement. The voltages v_{SU} and v_{U} in Fig. 2 are the oscilloscope measurements of the same source voltage waveform. Clearly, the high-impedance probe and oscilloscope do not exactly reproduce the voltage waveform v_{SU} generated by the source; the voltage waveform $20v_{\mathrm{U}}$ measured by the probe and oscilloscope differs in amplitude, shape, and time delay[1] from that generated by the source.

The observed differences between these measured voltage waveforms are primarily due to the nonideal transfer function of the high-impedance probe and electrical mismatches between the high-impedance probe and oscilloscope. The calibration method we developed corrects for these effects, as well as for the finite impulse response of the oscilloscope and for the oscilloscope's time-base distortion. The calibration measures the correct voltage waveforms both on the wafer and at the coaxial ports.

[1]In this case, the error in the time delay, which is attributable to the neglect of the electrical length of the high-impedance probe shown in Fig. 3(b), is somewhat greater than a single period of the waveform.

IV. On-Wafer Waveform Calibration

To calibrate waveforms measured with the high-impedance probe, we used both oscilloscope calibrations and mismatch corrections. We used the procedure in [9] to correct for the time-base distortion in the oscilloscope, and the swept-sine calibration of [10] to correct for the oscilloscope's amplitude response. The swept-sine calibration is based on injecting sine waves of known amplitudes into the coaxial input of the oscilloscope to characterize its amplitude response, and is traceable to power measurements. We then used the "nose-to-nose" calibration [11], [12], as implemented in [10] to calibrate the phase response of the oscilloscope. Finally, we measured the scattering parameters of the cable attached to the oscilloscope and moved the reference plane of the oscilloscope calibration to the end of the short coaxial cable at reference plane b in Fig. 1(a). After these calibrations, we calculate the frequency-domain voltage $V_{\mathrm{OSC}}(f)$ from the uncalibrated voltage $v_{\mathrm{U}}(t)$ measured by the scope. The voltage $V_{\mathrm{OSC}}(f)$ is the voltage that would be generated by the source across a perfect 50-Ω load at the coaxial reference plane b of Fig. 1(b) if the source had a perfect 50-Ω output impedance, as explained in [10].

We also developed an extensive frequency-domain probe mismatch correction. We used procedure A of [1] to characterize the probes because the conventional two-tier fixture characterization scheme [13] fails for lossy probes [1]. The corrections account for distortion due to the nonideal transfer function of the high-impedance probe and multiple reflections between the probe and oscilloscope.

The procedure outlined in [1] begins with a conventional two-tier characterization of the two 50-Ω GSG probes in Fig. 3(a). We started with a first-tier sliding-load short-open-load-thru (SOLT) vector network analyzer (VNA) calibration at coaxial reference planes indicated in Fig. 3. We then performed a second-tier on-wafer multiline thru-reflect

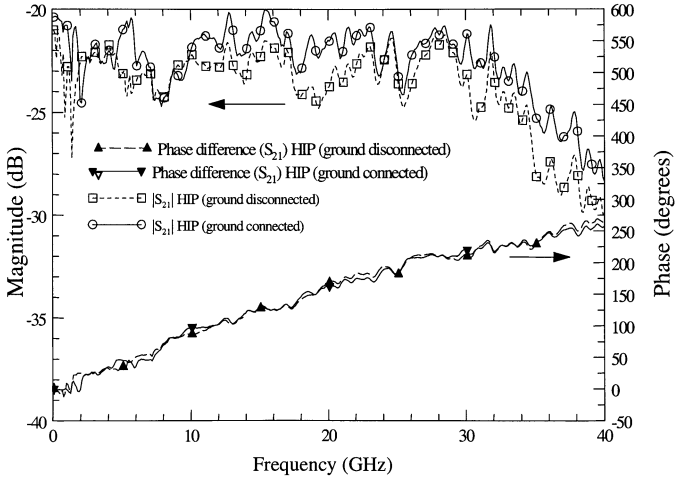

Fig. 4. Magnitude and phase of the transmission coefficient of the high-impedance probe with its ground connected (solid line) and disconnected (dashed line). We subtracted a time delay of 0.66 ns from the measurements to better illustrate the deviation from linear phase.

line (TRL) calibration [14] with reference impedance correction [15] based on a transmission-line capacitance determined from the measurement of a lumped resistor embedded in the line [16]. The artifacts we used in the second-tier on-wafer calibration consisted of CPW transmission lines 20.195-, 7.065-, 3.7-, and 2.635-mm long, a 0.5-mm-long CPW thru, and a symmetric CPW reflect printed on GaAs substrate. The reference plane for this on-wafer calibration was initially set in the center of the thru standard, but we moved the reference plane on port 1 to a position 25 μm from the right-most end of the thru line.

This two-tier calibration procedure measures a pair of electrical "error boxes" relating the coaxial and on-wafer calibrations to each other. Since the two calibration reference planes were physically separated by the probe and a short section of CPW line, the error boxes describe the electrical parameters of the 50-Ω GSG probes and section of CPW transmission line we wished to characterize. As a result, the port 1 error box of the second-tier calibration describes the electrical characteristics of the GSG probe at port 1 and the section of CPW line between it and the end of the thru.

Finally, we replaced the 50-Ω GSG probe at port 2 with the high-impedance probe that we wished to characterize, as illustrated in Fig. 3(b). We then measured the cascade of the GSG and high-impedance probe at the coaxial reference planes with the SOLT calibration. We finished by deembedding (subtracting) the electrical characteristics of the GSG probe and thru line characterized earlier, yielding the scattering parameters of the high-impedance probe. This completed the high-impedance probe characterization procedure A of [1]. As demonstrated in [1], the alternative probe characterization procedure B of [1] would have yielded similar results.

Fig. 4 shows typical measurements of the magnitude and phase of the forward transmission coefficient of the high-impedance probe. The solid lines in the figures correspond to measurements with the ground contact of the high-impedance probe attached to the ground plane of the CPW transmission line, while the dashed lines represent the measurements with the high-impedance probe ground contact disconnected. We found that these differences were quite important, and could not be neglected in the development of the calibration.

V. Mismatch Correction

Referring again to Fig. 1(a), which sketches the experimental apparatus, the objective of the mismatch correction was to correct for the nonideal transfer function of the high-impedance probe, as well as for multiple reflections between the probe and oscilloscope, on the measurements. To do this, we used an approach similar to those used in [17] and [18].

Fig. 1(b) shows an electrical block diagram of the experimental apparatus. For completeness, we included the equivalent circuits of both the source and oscilloscope. In this figure, $V_{\rm T}(f)$ is the Fourier transform of the voltage $v_{\rm T}(t)$ on the wafer we wish to measure, $V'_{\rm OSC}$ is the actual voltage at the coaxial reference plane b of Fig. 1(a) (not to be confused with $V_{\rm OSC}$, the voltage measured by the oscilloscope after it is calibrated to test devices with a 50-Ω input impedance [10]), $Z_{\rm S}(f)$ is the Thévenin equivalent impedance of the source corresponding to its reflection coefficient $\Gamma_{\rm S}(f)$ at the coaxial reference plane a of Fig. 1(a), $\Gamma_{\rm OSC}(f)$ is the reflection coefficient of the oscilloscope's sampling head at the coaxial reference plane b of Fig. 1(b), and $S_{\rm HIP}(f)$ are the scattering parameters of the high-impedance probe we determined from the procedure of [1].

From Kirchhoff's laws and the well-known relations between the input and output waves for the scattering-parameter matrix circuit description, we calculated the voltage $V_{\rm T}(f)$ from the voltage $V_{\rm OSC}(t)$ measured by the calibrated oscilloscope. After some algebraic manipulation, we derived a compact expression relating these two voltages. The expression is

$$V_{\rm T}(f) = V_{\rm OSC}(f)\big(\delta_1(f) + \delta_2(f)\big) \tag{1}$$

where

$$\delta_1(f) = \frac{1 - S_{22\rm HIP}(f)\cdot\Gamma_{\rm OSC}(f)}{S_{21\rm HIP}(f)} \tag{2}$$

and

$$\delta_2(f) = S_{11\rm HIP}(f)\cdot\delta_1(f) + S_{21\rm HIP}(f)\cdot\Gamma_{\rm OSC}(f) \tag{3}$$

and $V_{\rm OSC}(f)$ is the Fourier transform of the voltage $v_{\rm OSC}(t)$ that the source would deliver to the oscilloscope at reference plane b in Fig. 1(b) if the input impedance of the oscilloscope and cable was 50 Ω. Finally, we took the inverse Fourier transform of $V_{\rm T}(f)$ to determine the voltage $v_{\rm T}(t)$ at the end of the CPW transmission line.

VI. Measurement Results

Fig. 5 compares our on-wafer measurement of the voltage waveform $v_{\rm T}(t)$ calibrated with the procedure described in the last section with the ground of the high-impedance probe both connected to and disconnected from the CPW ground.

We also predicted the voltage $v_{\rm T}(t)$ on the wafer from a direct measurement of the source at the coaxial reference plane

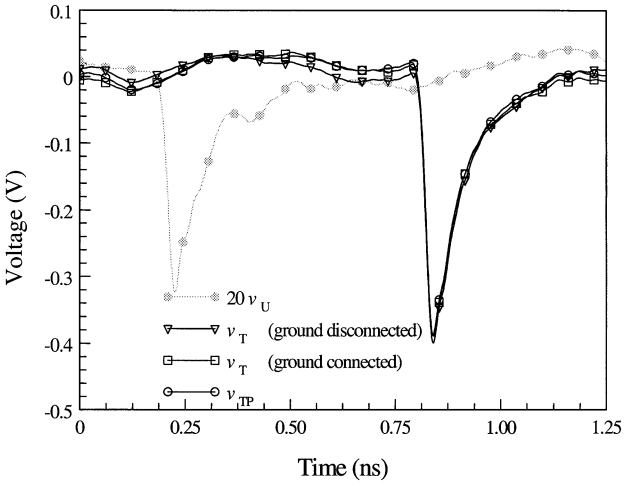

Fig. 5. On-wafer waveforms measured at the tip of the high-impedance probe. The waveform $v_{\mathrm{TP}}(t)$ is calculated from the measured characteristics of the source. The calibrated waveforms $v_{\mathrm{T}}(t)$ are determined with the procedure presented in the text. The waveform $20v_{\mathrm{U}}(t)$ is uncalibrated.

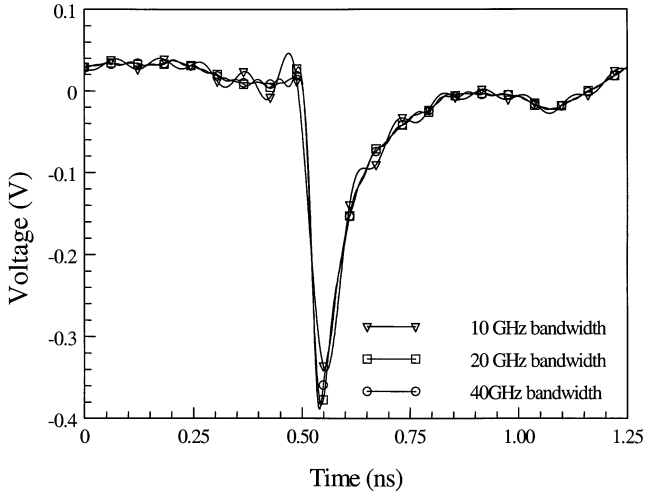

Fig. 6. Comparison of waveforms at the tip of high-impedance probe calibrated with the full 40-GHz bandwidth, truncated at 20 GHz and truncated at 10 GHz.

a of Fig. 1(a) using our calibrated oscilloscope and a measurement of the reflection coefficient of the source. This allowed us to determine the Thévenin equivalent voltage and resistance of the coaxial source. We then used the scattering parameters of the 50-Ω GSG probe and the CPW transmission line on the left-hand side of Fig. 1(a), as determined from the first step of the procedure described in [1], to calculate the waveform $v_{\mathrm{TP}}(t)$ on the wafer from the model of the source. Fig. 5 shows that the corrected measurements of $v_{\mathrm{T}}(t)$ also agree well with the prediction $v_{\mathrm{TP}}(t)$, showing that the calibration presented here accurately determines the voltage waveform in the CPW line.

Fig. 5 also plots the voltage $20v_{\mathrm{U}}(t)$, the uncalibrated waveform $v_{\mathrm{U}}(t)$ measured by the oscilloscope and multiplied by 20, the expected factor for this 20× high-impedance probe with a 950-Ω resistor integrated into the tip. Not only does this uncalibrated measurement show the pulse arriving at the wrong time, but also the measured peak voltage and details of the pulse shape are incorrect. This illustrates the significant improvement in accuracy obtained with the calibration procedure proposed here.

VII. Discussion and Limitations

The reference plane at which the high-impedance probe and oscilloscope measure v_{T} is determined during the scattering-parameter characterization of the probe used in the procedure of [1] and is set by the on-wafer CPW TRL calibration to a reference plane 25 μm from the right-hand-side end of the CPW. As a result, the measured v_{T} is a well-defined voltage in the CPW transmission line.

However, it is important to keep in mind that v_{T} is not actually measured at the tip of the high-impedance probe, where the voltage may not always be well defined. In fact, the scattering-parameter matrix S_{HIP} we used to perform the mismatch corrections includes the high-impedance probe, its connection parasitics, and the 25-μm section of CPW under the probe and its fringing capacitance. Reference [19] shows that these on-wafer calibrations are specific to the particular CPW lines in which they are developed, and are not universally applicable to other transmission lines and measurement situations.

We also found that the differences in the electrical behavior of the probes with the ground connected and disconnected were not negligible. While not shown in the figures, we found that, if we used a mismatch correction with the ground disconnected to correct measurement performed with the ground connected, or vice versa, the error in measuring v_{T} increased significantly. Again, we see that the calibration is a custom calibration that should be performed in the specific test environment in which the probes are to be used to give the best results.

VIII. Calibration Bandwidth

Since our calibration scheme depends on frequency-domain mismatch corrections, the finite bandwidth of the correction results in some degradation of the waveform. In our experiment, the power from the source fell from its maximum value at 800 MHz by 12 dB at 10 GHz, 24 dB at 20 GHz, and 40 dB at 40 GHz. As a result, we expected that our 40-GHz calibration bandwidth would be adequate for characterizing v_{T}.

To test for this, we reduced the bandwidth of the corrections to 20 and 10 GHz. Fig. 6 compares the results. This figure shows that, while truncating the measurement bandwidth at 10 GHz introduced significant ripple on the waveform, truncating the measurement bandwidth at 20 GHz introduces only small ripples. From this, we concluded that our 40-GHz measurement bandwidth was indeed adequate in our experiments.

We also found that the impact of the mismatch corrections in our measurement system (and the time–base-distortion correction, which is needed to obtain accurate mismatch corrections) on the overall accuracy of the waveform measurements was much greater than the impact of the oscilloscope calibration. We attribute this to the fact that our oscilloscope response was quite flat to 20 GHz so the corresponding swept-sine and nose-to-nose corrections were quite small, below 20 GHz where most of the signal energy was present.

IX. Conclusions

We introduced a calibration technique for the measurement of on-wafer voltage waveforms with noninvasive internal-node probes. We demonstrated this technique on commercially available high-impedance probes, and showed that these probes can be used both with and without a ground connection with comparable results.

Acknowledgment

The authors thank T. S. Clement, P. Hale, K. J. Coakley, and C.-M. Wang, all of the National Institute of Standards and Technology (NIST), Boulder, CO, for performing the oscilloscope calibrations.

References

[1] U. Arz, H. C. Reader, P. Kabos, and D. F. Williams, "Wideband frequency-domain characterization of high-impedance probes," in *58th ARFTG Conf. Dig.*, San Diego, CA, Nov. 2001.

[2] K. Yang, L. P. B. Katehi, and J. F. Whitaker, "Electro-optic field mapping system utilizing external gallium–arsenide probes," *Appl. Phys. Lett.*, vol. 77, pp. 486–488, 2000.

[3] M. D. Weiss, M. H. Crites, E. W. Bryerton, J. F. Whitaker, and Z. Popović, "Time-domain optical sampling of switched mode microwave amplifiers and multipliers," *IEEE Trans. Microwave Theory Tech.*, vol. 47, pp. 2599–2604, Dec. 1999.

[4] S. Kono, M. Tani, and K. Sakai, "Ultrabroadband photoconductive detection: Comparison with free space electro-optic sampling," *Appl. Phys. Lett.*, vol. 79, pp. 898–900, 2001.

[5] T. Nagatsuma, M. Shinagava, N. Sahri, A. Sasaki, Y. Royter, and A. Hirata, "1.55-μm photonic systems for microwave and millimeter-wave measurements," *IEEE Trans. Microwave Theory Tech.*, vol. 49, pp. 1831–1839, Oct. 2001.

[6] D. W. van der Weide, "Localized picosecond resolution with a near-field microwave/scanning-force microscope," *Appl. Phys. Lett.*, vol. 70, pp. 677–679, 1997.

[7] C. J. Wei, Y. A. Tkachenko, J. C. M. Hwang, K. E. Smith, and A. H. Peake, "Internal-node waveform probing of MMIC power amplifiers," in *IEEE Microwave and Millimeter Wave Monolithic Circuits Symp.*, 1995, pp. 127–130.

[8] J. C. M. Hwang, "Internal waveform probing of MMIC power amplifiers," in *Proc. 2nd Int. Microwave and Millimeter Wave Technology Conf.*, 2000, pp. 638–641.

[9] C. M. Wang, P. D. Hale, and K. J. Coakley, "Least-squares estimation of time-base distortion of sampling oscilloscopes," *IEEE Trans. Instrum. Meas.*, vol. 48, pp. 1324–1332, Dec. 1999.

[10] P. D. Hale, T. S. Clement, K. C. Coakley, C. M. Wang, D. C. DeGroot, and A. P. Verdoni, "Estimating the magnitude and phase response of a 50 GHz sampling oscilloscope using the 'nose-to-nose' method," in *55th ARFTG Conf. Dig.*, June 2000.

[11] J. Verspecht and K. Rush, "Individual characterization of broadband sampling oscilloscopes with a nose-to-nose calibration procedure," *IEEE Trans. Instrum. Meas.*, vol. 43, pp. 347–354, Apr. 1994.

[12] K. Rush, S. Draving, and J. Kerley, "Characterizing high-speed oscilloscopes," *IEEE Spectr.*, pp. 38–39, Sept. 1990.

[13] R. F. Bauer and P. Penfield, "De-embedding and unterminating," *IEEE Trans. Microwave Theory Tech.*, vol. MTT-39, pp. 282–288, 1974.

[14] R. B. Marks, "A multiline method of network analyzer calibration," *IEEE Trans. Microwave Theory Tech.*, vol. 39, pp. 1205–1215, July 1991.

[15] R. B. Marks and D. F. Williams, "Characteristic impedance determination using propagation constant measurement," *IEEE Microwave Guided Wave Lett.*, vol. 1, pp. 141–143, June 1991.

[16] D. F. Williams and R. B. Marks, "Transmission line capacitance measurement," *IEEE Microwave Guided Wave Lett.*, vol. 1, pp. 243–245, Sept. 1991.

[17] D. F. Williams, P. D. Hale, T. S. Clement, and J. M. Morgan, "Mismatch corrections for electro-optic sampling systems," in *56th ARFTG Conf. Dig.*, Nov. 30–Dec. 1, 2000, pp. 141–145.

[18] P. D. Hale, T. S. Clement, D. F. Williams, E. Balta, and N. D. Taneja, "Measuring the frequency response of gigabit chip photodiodes," *J. Lightwave Technol.*, vol. 19, pp. 1333–1339, Sept. 2001.

[19] D. F. Williams and R. B. Marks, "Compensation for substrate permittivity in probe-tip calibration," in *44th ARFTG Conf. Dig.*, Dec. 1994, pp. 20–30.

Pavel Kabos (SM'93) was born in Kosice, Czechoslovakia. He received the M.S. degree (with honors), and Ph.D. and Dr.Sc. degrees in applied physics (theoretical electrotechnique) from the Slovak Technical University, Bratislava, Slovakia, in 1972, 1979, and 1994, respectively.

In 1972, he joined the Department of Theoretical and Applied Electro-Technique, Slovak Technical University, as an Assistant Professor and, in 1983, became an Associate Professor. From 1982 to 1984, he held a post-doctoral position with Colorado State University (CSU). In December 1991, he joined the Magnetic Group, Department of Physics, CSU. In 1997, he joined the Magnetic Group, Electromagnetic Wave Technology Division, National Institute of Standards and Technology (NIST), Boulder, CO. Since August 2000, he has been with the RF Technology Division, NIST. He has authored and coauthored a book, several book chapters, and numerous publications in experimental high-frequency physics and electronics.

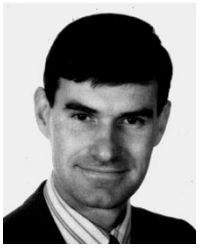

Howard Charles Reader was born in Johannesburg, South Africa, in 1959. He received the B.Sc. degree in electrical engineering (with first-class honors) from King's College London, London, U.K., in 1982, and the Doctorate degree from Cambridge University (St. John's College), Cambridge, U.K. His doctoral research concerned time-domain techniques for antenna analysis.

His doctoral studies incorporated a three-year collaboration with the Marconi Research Centre, Essex, U.K. From 1986 to 1994, he was a Lecturer, Senior Lecturer, and Associate Professor of electronic engineering with the University of Natal. In 1994, he became the Chair of High Frequency Electronics with the Electrical and Electronic Engineering Department, Stellenbosch University. His principal teaching, research, and industrial interests since 1986 have been in microwave dielectric heating, metrology, high-frequency circuits, and electromagnetic compatibility.

Dr. Reader is a Chartered Engineer in the U.K. He is a Member of the Institution of Electrical Engineers (IEE), U.K. (sitting on the Professional Network on Electromagnetics). He is chairman of South Africa's URSI Commission E (EMI).

Uwe Arz (S'97–M'02) received the Dipl.-Ing. degree in electrical engineering and Ph.D. degree (*summa cum laude*) from the University of Hannover, Hannover, Germany, in 1994 and 2001, respectively.

From 1995 to 2001, he was a Research and Teaching Assistant with the Laboratory of Information Technology, University of Hannover. In 2001 he was a Post-Doctoral Research Associate with the National Institute of Standards and Technology (NIST), Boulder, CO. In 2002, he joined the Physikalisch-Technische Bundesanstalt (PTB), Braunschweig, Germany, where he develops metrology for on-wafer measurements.

Dr. Arz was the recipient of the first ARFTG Microwave Measurement Fellowship Award.

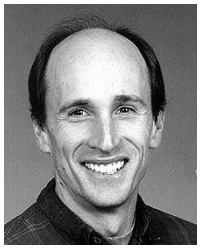

Dylan F. Williams (M'80–SM'90–F'02) received the Ph.D. degree in electrical engineering from the University of California at Berkeley, in 1986.

In 1989, he joined the Electromagnetic Fields Division, National Institute of Standards and Technology (NIST), Boulder, CO, where he develops metrology for the characterization of monolithic microwave integrated circuits and electronic interconnects. He has authored or coauthored over 80 technical papers.

Dr. Williams was the recipient of the Department of Commerce Bronze and Silver Medals, the Electrical Engineering Laboratory's Outstanding Paper Award, two ARFTG Best Paper Awards, the ARFTG Automated Measurements Technology Award, and the IEEE Morris E. Leeds Award.